Electronic Supplementary Material (ESI) for Physical Chemistry Chemical Physics

Structural Investigation of a Hydrogen Bond Order-Disorder Transition in a Polar One-Dimensional Confined Ice

SUPPLEMENTARY INFORMATION

Jasper Adamson, Nicholas P. Funnell, Amber L. Thompson, and Andrew L. Goodwin*

Department of Chemistry, University of Oxford, Inorganic Chemistry Laboratory,
South Parks Road, Oxford OX1 3QR, U.K.
*To whom correspondence should be addressed; E-mail: andrew.goodwin@chem.ox.ac.uk.

Submitted to Physical Chemistry Chemical Physics

Contents

1 Synthesis of HHTP·4H_2O

Powdered HHTP·H_2O was obtained from Tokyo Chemical Industry UK. Successive recrystallisations from acetone and a 1:1 volume mixture of water and acetone, yielded dark red needle-like crystals from slow evaporation. The crystal habit is illustrated in Fig. S1.

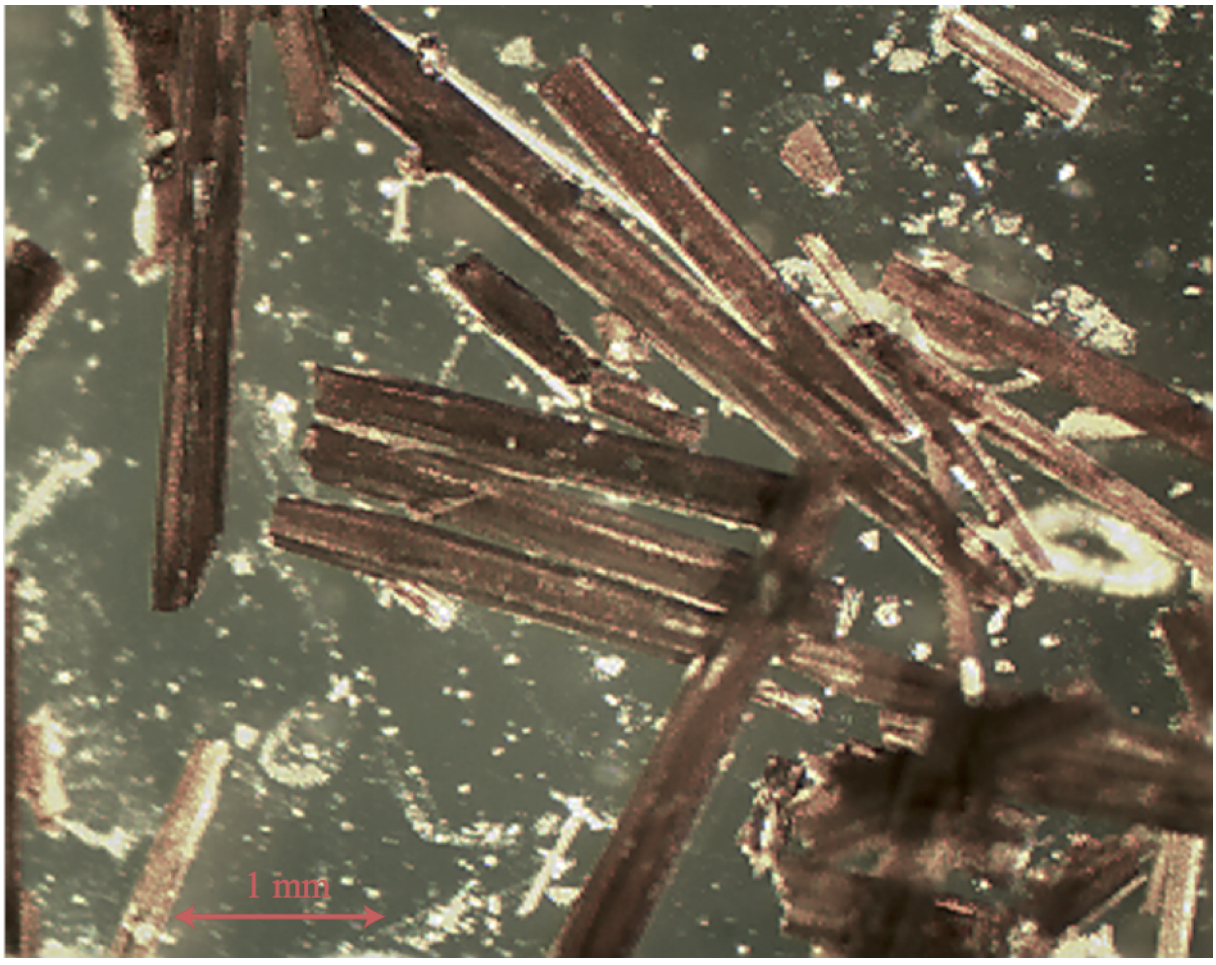

Figure S1: Optical microscopy image of representative crystals of HHTP·4H_2O, prepared as described in the main text. The crystal habit is rectangular prismatic, with the long axis parallel to the $\mathbf{c}$ crystal axis (*i.e.*, the confinement axis).

2 Variable-temperature single crystal X-ray diffraction

2.1 Method

X-ray diffraction data were collected on a single crystal of HHTP·4H_2O using an Oxford Diffraction (Agilent Technologies) SuperNova (Mo Kα radiation) equipped with an Oxford Cryosystems cryostream.[S1] The sample was coated in perfluoropolyether oil and placed in the cold N_2 open flow of an Oxford CryoSystems Cryostream[S1] at 100 K, after data were collected on heating the sample to 240 K in 10 K intervals. The crystal was then heated to 260 K to ensure the sample had undergone complete transformation, before it was cooled to 240 K. Subsequent data collections between 240 and 130 K were also carried out. Data were integrated and corrected for absorption using CrysAlisPro. The structure was solved using the data collected at 100 K, using SIR92[S2] and refined against F^2 using full-matrix least squares, as implemented in CRYSTALS.[S3] All non-hydrogen atoms in the 100 K structure were refined with anisotropic displacement parameters. Hydrogen atoms were visible in the difference map and positioned as given in Section 2.2. At 240 K, only the non-hydrogen atoms bound to the HHTP moiety were refined with anisotropic displacement parameters; water oxygens were split over two sites and refined with isotropic displacement parameters, with partial occupancies of 50%. Hydrogen atoms in both structures were located using a difference Fourier map — detailed information on the treatment of hydrogen atoms is given further below. Select crystal structure refinement details are given in Tables S1 and S2. Variable-temperature lattice parameters are given in Tables S3 and S4; the corresponding trends are illustrated in Fig. S2.

The conventions for placing the unit cell origin differ between the space groups $Pbcn$ and $P2_1cn$. In order to facilitate direct comparison of the atomic coordinates, we have implemented an origin shift for the $P2_1cn$ structure solution (100 K). This choice of nonstandard origin generates a number of alerts in checkCIF; these can safely be ignored.

Table S1: Single-crystal X-ray diffraction data collection and refinement details for HHTP·4H_2O at $T = 100$ K on heating.

Radiation	Mo $K\alpha$, $\lambda = 0.71073$ Å
Formula	$C_{18}H_{20}O_{10}$
M, g mol^{-1}	396.35
Z	4
Crystal Size (mm)	0.03 × 0.10 × 0.19
Crystal System	Orthorhombic
Space Group	$P2_1cn$
a (Å)	14.20002(19)
c (Å)	16.7353(2)
c (Å)	7.17809(9)
V (Å^3)	1705.82(4)
No. of Reflections($I/\sigma > 2.0$)	3455
Goodness of Fit	1.0051
$R(I/\sigma > 2.0)$	0.0308

Atom	x	y	z	U_{eq}, Å^2
C1	0.45532(13)	0.26668(9)	0.7171(2)	0.0156
C2	0.41227(14)	0.33799(9)	0.67410(18)	0.0152
C3	0.45536(13)	0.41202(8)	0.7117(2)	0.0127
C4	0.40722(13)	0.48741(9)	0.66958(18)	0.0137
C5	0.31699(12)	0.48968(9)	0.58813(19)	0.0136
C6	0.27207(12)	0.56128(11)	0.5536(2)	0.0157
C7	0.31614(12)	0.63329(9)	0.6011(2)	0.0150
C8	0.40401(13)	0.63238(10)	0.68049(19)	0.0157
C9	0.45232(12)	0.55999(9)	0.7129(2)	0.0130
C10	0.54698(12)	0.56069(9)	0.7904(2)	0.0140
C11	0.59399(14)	0.63291(9)	0.82159(19)	0.0152

Continued on next page

Table S1 – continued from previous page

Atom	x	y	z	U_{eq}, Å^2
C12	0.68197(13)	0.63534(9)	0.8980(2)	0.0155
C13	0.72726(12)	0.56368(10)	0.9493(2)	0.0146
C14	0.68288(13)	0.49212(9)	0.9154(2)	0.0148
C15	0.59224(14)	0.48820(8)	0.83422(19)	0.0126
C16	0.54572(13)	0.41266(9)	0.7943(2)	0.0133
C17	0.58911(14)	0.33872(8)	0.83568(19)	0.0145
C18	0.54533(13)	0.26732(9)	0.7981(2)	0.0155
O1	0.41568(10)	0.19318(7)	0.68496(18)	0.0229
O6	0.18498(10)	0.56655(6)	0.47125(17)	0.0192
O7	0.26846(10)	0.70355(7)	0.56481(17)	0.0199
O12	0.72914(10)	0.70638(7)	0.93153(17)	0.0195
O13	0.81367(10)	0.57082(6)	1.03129(17)	0.0200
O18	0.58427(11)	0.19421(6)	0.83644(16)	0.0209
O100	−0.07227(11)	0.55742(9)	0.5735(2)	0.0304
O200	−0.11545(12)	0.67420(8)	1.30833(18)	0.0319
O300	0.10297(12)	0.66840(8)	1.21325(17)	0.0306
O400	0.08209(12)	0.56316(8)	0.9234(2)	0.0311
H11	0.3602	0.1971	0.6563	0.0352
H21	0.3526	0.3370	0.6185	0.0177
H51	0.2863	0.4426	0.5547	0.0156
H61	0.1600	0.5234	0.4498	0.0311
H71	0.3052	0.7414	0.5855	0.0314
H81	0.4311	0.6819	0.7111	0.0182
H111	0.5658	0.6826	0.7869	0.0171
H121	0.7011	0.7425	0.8696	0.0303
H131	0.8359	0.5278	1.0619	0.0306
H141	0.7134	0.4444	0.9501	0.0178
H171	0.6509	0.3383	0.8921	0.0170

Continued on next page

Table S1 – continued from previous page

Atom	x	y	z	U_{eq}, Å^2
H181	0.6372	0.1984	0.8850	0.0325
H1001	−0.0523	0.5894	0.6524	0.0484
H1002	−0.0205	0.5357	0.5320	0.0472
H2001	−0.1494	0.6542	1.2217	0.0504
H2002	−0.1002	0.6417	1.3946	0.0502
H3001	0.1314	0.6452	1.3042	0.0464
H3002	0.0475	0.6725	1.2555	0.0471
H4001	0.0922	0.5916	0.8282	0.0480
H4002	0.0803	0.5887	1.0241	0.0479

Estimated standard deviations are given in parentheses.

Table S2: Single-crystal X-ray diffraction data collection and refinement details for HHTP·4H_2O at $T = 240$ K on heating.

Space Group	$Pbcn$			
a (Å)	14.2568(2)			
b (Å)	16.7791(2)			
c (Å)	7.2308(1)			
V (Å^3)	1729.73(4)			
No. of Reflections($I/\sigma > 2.0$)	1609			
Goodness of Fit	0.9963			
$R(I/\sigma > 2.0)$	0.0487			
Atom	x	y	z	U_{eq}, Å^2
C1	0.45531(11)	0.26762(9)	0.7101(2)	0.0287
C2	0.41209(11)	0.33865(9)	0.6705(2)	0.0267
C3	0.45487(10)	0.41240(8)	0.7092(2)	0.0226
C4	0.40783(10)	0.48771(9)	0.66921(19)	0.0225
C5	0.31771(10)	0.49067(9)	0.5894(2)	0.0257
C6	0.27303(11)	0.56190(9)	0.5557(2)	0.0275
C7	0.31717(11)	0.63343(9)	0.6044(2)	0.0283
C8	0.40490(11)	0.63196(9)	0.6803(2)	0.0278
C9	0.45277(10)	0.56006(9)	0.7117(2)	0.0235
O1	0.41629(9)	0.19451(7)	0.6751(2)	0.0437
O6	0.18630(9)	0.56766(7)	0.4754(2)	0.0384
O7	0.26947(8)	0.70354(7)	0.5698(2)	0.0384
O100	−0.0671(3)	0.5590(3)	0.5476(6)	0.0558(12)
O200	−0.1287(3)	0.6728(2)	1.3105(5)	0.0534(10)
O300	−0.0997(3)	0.6703(2)	1.2830(5)	0.0458(8)
O400	−0.0838(3)	0.5616(2)	0.5923(6)	0.0466(10)
H21	0.3534	0.3384	0.6154	0.0287

Continued on next page

Table S2 – continued from previous page

Atom	x	y	z	U_{eq}, Å^2
H51	0.2892	0.4447	0.5538	0.0288
H81	0.4330	0.6795	0.7127	0.0312
H11	0.3654	0.1974	0.6341	0.0633
H61	0.1668	0.5263	0.4328	0.0532
H71	0.2989	0.7372	0.6232	0.0564
H1001	−0.0642	0.5858	0.6435	0.0763
H1002	−0.0162	0.5381	0.5158	0.0758
H2001	−0.1489	0.6481	1.2185	0.0721
H2002	−0.0994	0.6467	1.3865	0.0713
H3001	−0.1446	0.6692	1.2044	0.0649
H3002	−0.0478	0.6651	1.2312	0.0651
H4001	−0.1234	0.5859	0.6559	0.0644
H4002	−0.0709	0.5844	0.4924	0.0638

Estimated standard deviations are given in parentheses.

Table S3: Temperature dependence of unit cell parameters (heating).

Temperature (K)	**a** (Å)	**b**(Å)	**c**(Å)	V(Å^3)
100	14.20002(19)	16.7353(2)	7.17809(9)	1705.82(4)
110	14.20532(15)	16.73488(19)	7.18143(7)	1707.20(3)
120	14.21093(16)	16.7346(2)	7.18522(8)	1708.75(3)
130	14.21481(15)	16.73492(19)	7.18961(8)	1710.29(3)
140	14.21987(16)	16.7376(2)	7.19397(8)	1712.21(3)
150	14.22557(16)	16.7401(2)	7.19826(8)	1714.18(3)
160	14.22928(16)	16.7414(2)	7.20240(8)	1715.74(3)
170	14.23442(16)	16.7428(2)	7.20560(8)	1717.27(3)
180	14.23847(15)	16.74459(19)	7.20989(8)	1718.96(3)
190	14.24309(16)	16.7493(2)	7.21389(8)	1720.96(3)
200	14.24638(16)	16.7531(2)	7.21670(8)	1722.42(3)
210	14.24903(15)	16.75843(19)	7.22030(8)	1724.14(3)
220	14.25171(15)	16.76451(19)	7.22359(8)	1725.88(3)
230	14.25477(16)	16.7711(2)	7.22697(9)	1727.74(4)
240	14.2568(2)	16.7793(2)	7.2308(1)	1729.73(4)

Table S4: Temperature dependence of unit cell parameters (cooling).

Temperature (K)	**a** (Å)	**b**(Å)	**c**(Å)	V(Å^3)
240	14.2551(3)	16.7783(4)	7.23216(18)	1729.76(8)
230	14.2521(3)	16.7712(4)	7.22817(18)	1727.71(8)
220	14.2508(4)	16.7653(4)	7.22435(18)	1726.04(8)
210	14.2512(4)	16.7650(4)	7.22398(18)	90.005(2)
200	14.2517(4)	16.7647(4)	7.22358(18)	1725.90(8)
190	14.2448(4)	16.7449(5)	7.2121(2)	1720.30(8)
180	14.2429(4)	16.7414(4)	7.20818(19)	1718.76(8)
170	14.2399(4)	16.7372(4)	7.2040(2)	1716.96(8)
160	14.2380(4)	16.7327(4)	7.2006(2)	1715.47(8)
150	14.2352(4)	16.7291(5)	7.1962(2)	1713.73(9)
140	14.2332(4)	16.7263(5)	7.1923(2)	1712.26(9)
130	14.2312(4)	16.7237(5)	7.1880(2)	1710.73(9)

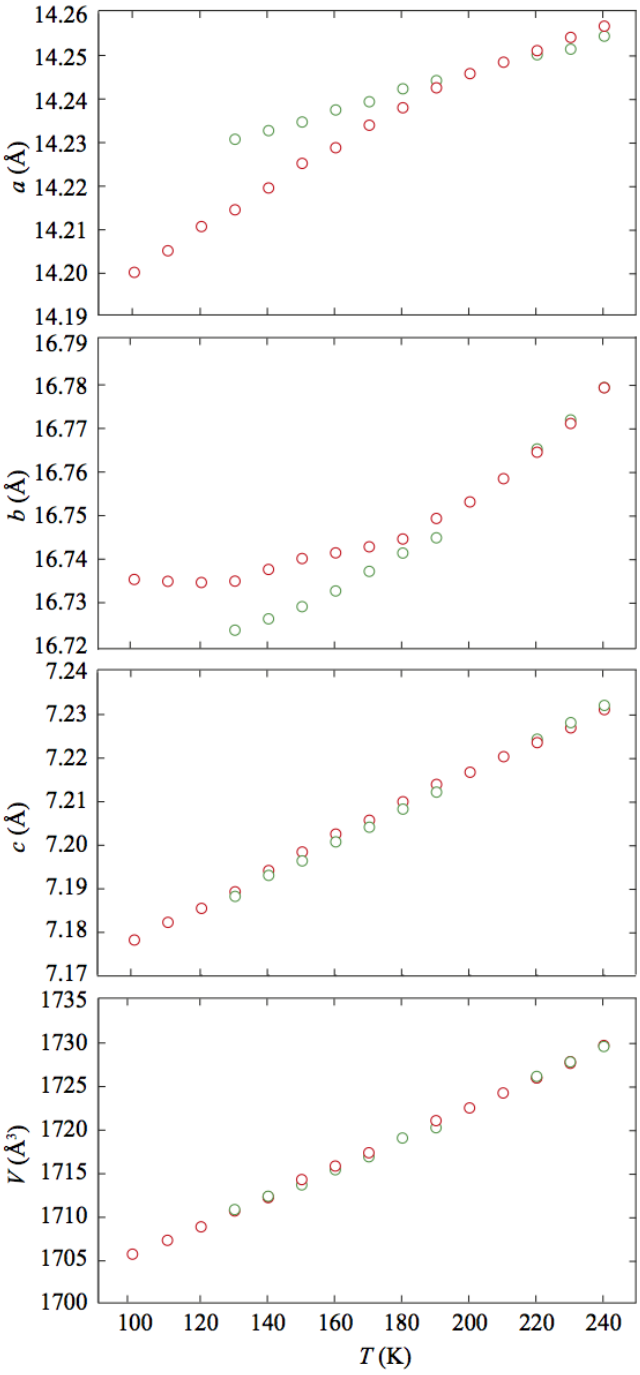

Figure S2: Thermal dependence of the lattice parameters, indicating the lack of hysteresis on cooling. Red circles represent the heating and green circles the cooling data. The deviation at low temperatures observed for the **a** and **b** axes is likely attributable to partial dehydration of the framework after sustained exposure to dry N_2 gas.

2.2 Treatment of water molecules

Particular care was given to hydrogen atom placement owing to the disordered nature of the water channel sub-structure, described in the manuscript. For the 100 K dataset, following initial anisotropic refinement of non-hydrogen atoms, all hydrogen atoms were located using a difference Fourier map. Hydrogen atom positions and isotropic thermal parameters were refined with soft restraints prior to their inclusion in the final refinement using a riding model (as described in Ref. 4).

Scattering by hydrogen atoms makes a larger relative contribution to low angle reflection intensities owing to a greater fall-off in scattered intensity than that of non-hydrogen atoms (see Fig. 5 in Ref. 4). Thus, truncating the data to lower resolutions has the effect of enhancing the electron density attributed to hydrogen atoms (1.1 Å has been identified as a suitable cut-off). Figure S3(a) shows a generalised difference Fourier section calculated in the vicinity of the water molecules using the data below 1.1 Å, when the occupancies of the water hydrogens are set to zero. For all four molecules, there are clearly defined regions of density for each of the hydrogens.

A similar procedure was followed for the 240 K data, however the initial coordinates of the water molecules were derived from the ordered, low temperature structure. The b-glide symmetry operator, not present at 100 K, collapses the four water molecules onto two positions, resulting in a superposition of the two water channel meso-helices (O400 maps onto O100, and O300 onto O200), thus each water molecule is half occupied. Refinement of the oxygen with anisotropic thermal parameters is unstable due to correlation caused by the close proximity of the two sites. Hydrogen atom positions and isotropic thermal parameters were then refined with soft restraints prior to their inclusion in the final refinement using a riding model as for the structure determined at 100 K. Figure S3(b) shows a generalised difference Fourier section when the hydrogen atom occupancies are set to zero.

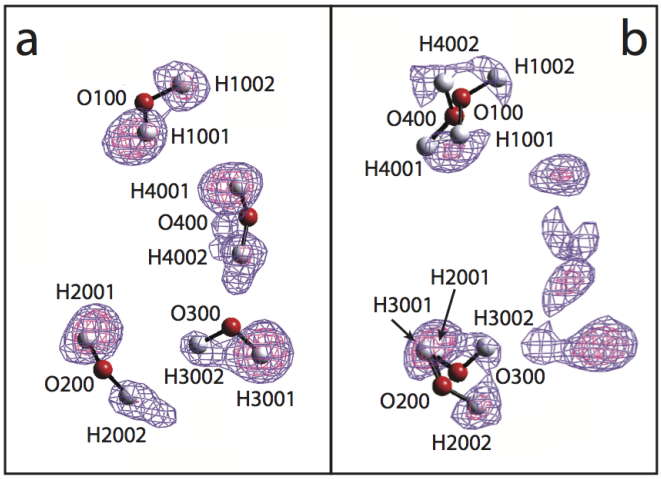

Figure S3: Generalised section of the difference Fourier maps for the water molecules with hydrogen occupancies set to 0 and the data truncated at 1.1 Å for (a) 100 K ($Pna2_1$) and (b) 240 K ($Pbcn$). The unoccupied density in (b) becomes symmetry-related to the other regions of density by the b-glide that is generated by the phase transition. When hydrogen occupancies are set to 1 (in (a)) and 0.5 (in (b)), no density is visible.

3 The order parameter

3.1 Relationship to diffraction intensities

The relevant order parameter for this order/disorder transition can be related directly from the structure factor expression. We consider the system to consist of fractions χ and $(1-\chi)$ of the low-temperature $P2_1cn$ structure and its inverse (obtained by action of a b-glide perpendicular to $\mathbf{a}$); the corresponding order parameter is consequently

$$\xi = 2\chi - 1. \tag{1}$$

Using this construction, the structure factor associated with $(0kl)$ reflections is

$$F(0kl) = \chi \sum_{j=1}^{N} f_j \exp[2\pi\mathrm{i}(ky_j + lz_j)] + (1-\chi) \sum_{j=1}^{N} f_j \exp\{2\pi\mathrm{i}[k(y_j + \frac{1}{2}) + lz_j]\}, \tag{2}$$

$$= \sum_{j=1}^{N} f_j \exp[2\pi\mathrm{i}(ky_j + lz_j)][\chi + (1-\chi)\exp(\pi\mathrm{i}k)]. \tag{3}$$

For those $(0kl)$ reflections forbidden in $Pbcn$ (*i.e.*, k odd), we have

$$F(0kl) = (2\chi - 1)F_{P2_1cn}(0kl), \tag{4}$$

where $F_{P2_1cn}(0kl)$ is the relevant structure factor for the ordered $P2_1cn$ phase. Consequently $I(0kl) = |F(0kl)|^2$ is proportional to ξ^2 and ξ to $\sqrt{I(0kl)}$.

3.2 Experimental determination of the order parameter variation with temperature

Measured intensities for three representative systematic absence violations and the reference (042) reflection are given in Table S5. The corresponding values of the order parameter xi and their uncertainties are given in Table S6; these results are plotted in Fig. S4. Synthesised precession images assembled from the raw diffraction data are shown in Fig. S5 in order to illustrate the disappearance and emergence of satellite reflections on heating and cooling.

Table S5: Selected reflection intensities, averaged over all symmetry equivalent reflections, for HHTP·4H_2O.

T (K)	I(042)	σ_I(042)	I(071)	σ_I(071)	I(031)	σ_I(031)	I(011)	σ_I(011)
100	28488	141	5345	81	763	21	1708	43
110	27580	139	5117	83	773	20	1687	41
120	28133	143	5195	83	789	20	1710	42
130	28433	148	5028	86	792	22	1652	43
140	28329	150	4922	78	780	22	1652	42
150	27562	147	4749	76	773	20	1562	41
160	28343	152	4759	78	796	21	1600	42
170	27993	149	4325	73	752	21	1514	40
180	28188	152	4063	73	693	21	1464	40
190	29205	160	3908	74	680	21	1419	41
200	29269	163	3464	71	597	22	1325	41
210	29772	166	2920	73	476	19	1080	39
220	31408	176	1994	64	365	19	790	36
230	31287	185	929	50	174	17	326	27
240	30318	175	152	29	39	14	74	19

Table S6: Order parameters for selected reflections for HHTP·4H_2O.

Temperature (K)	ξ(071)	σ_ξ(071)	ξ(031)	σ_ξ(031)	ξ(011)	σ_ξ(011)
100	0.4332	0.0034	0.1637	0.0023	0.2448	0.0031
110	0.4307	0.0037	0.1674	0.0022	0.2473	0.0031
120	0.4297	0.0036	0.1675	0.0022	0.2465	0.0031
130	0.4205	0.0038	0.1669	0.0023	0.2410	0.0032
140	0.4168	0.0035	0.1659	0.0024	0.2415	0.0032
150	0.4151	0.0035	0.1674	0.0023	0.2380	0.0032
160	0.4098	0.0035	0.1676	0.0023	0.2376	0.0032
170	0.3931	0.0035	0.1639	0.0023	0.2325	0.0031
180	0.3797	0.0035	0.1568	0.0024	0.2279	0.0032
190	0.3658	0.0036	0.1526	0.0024	0.2204	0.0032
200	0.3440	0.0037	0.1428	0.0026	0.2128	0.0034
210	0.3132	0.0040	0.1264	0.0026	0.1904	0.0035
220	0.2520	0.0041	0.1078	0.0029	0.1586	0.0037
230	0.1723	0.0047	0.0745	0.0036	0.1021	0.0042
240	0.0707	0.0067	0.0361	0.0063	0.0495	0.0063

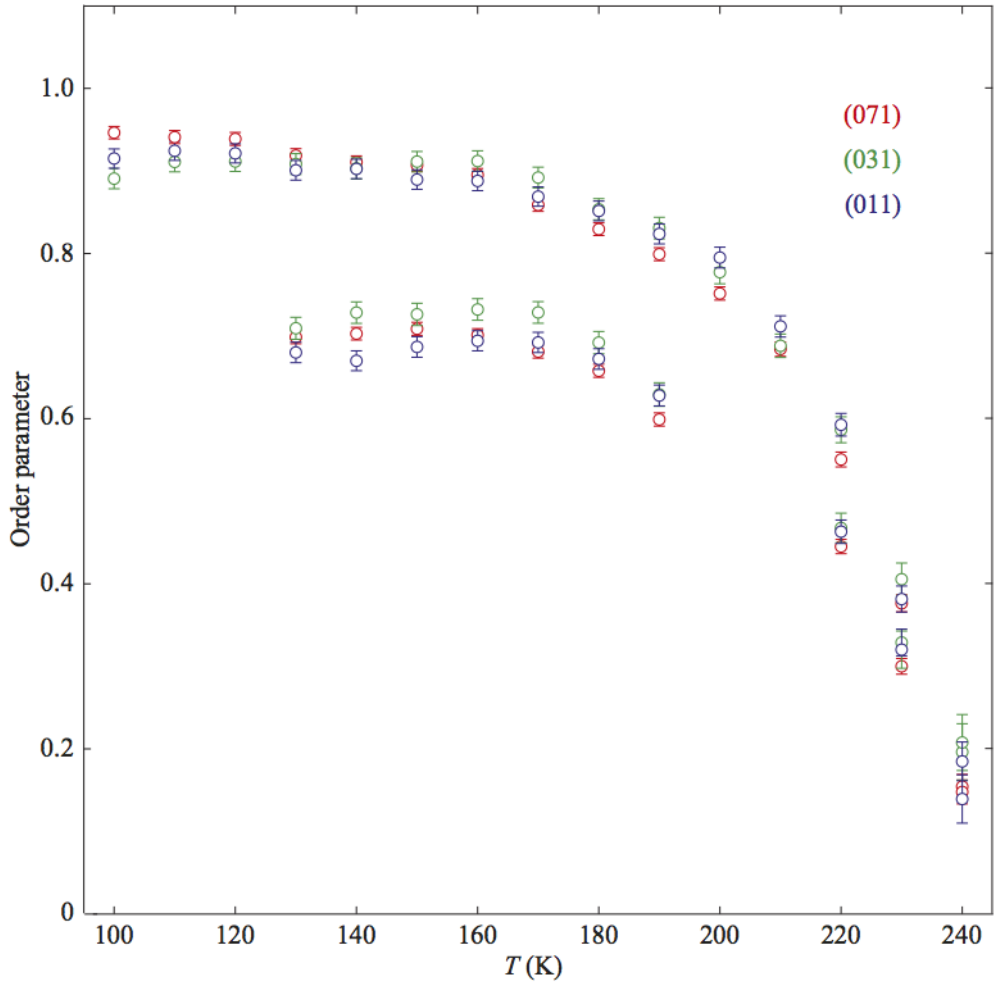

Figure S4: Thermal dependence of the order parameter plot, indicating the lack of hysteresis on cooling. The discrepancy between the values of the order parameter at low temperature between heating and cooling runs is discussed in the main text.

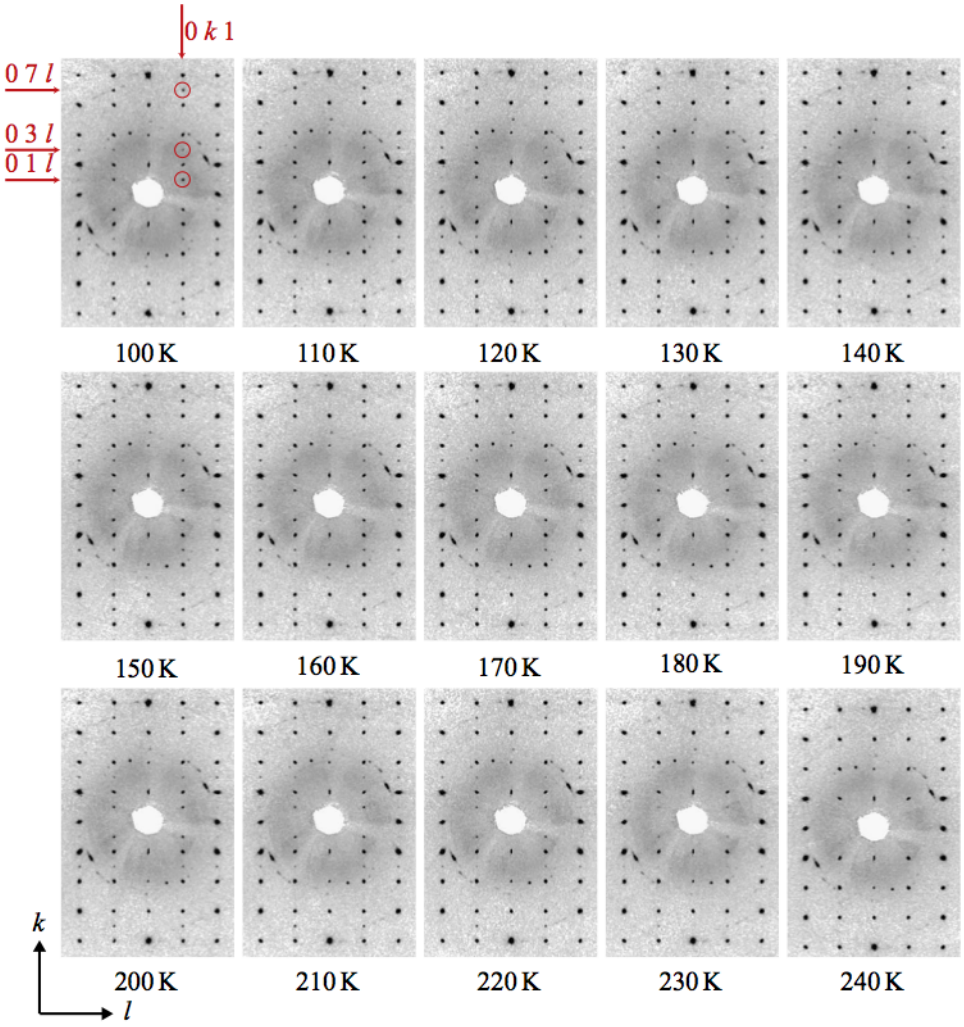

Figure S5: Synthesised precession images of the $(0kl)$ plane, showing the decay of systematic absence violations for $Pbcn$. The systematic absences visible for the (071), (031) and (011) reflections are denoted with red circles on the 100 K image. Their intensities decrease with temperature and are completely absent by 240 K.

4 References

(S1) J. Cosier, A. Glazer, *J. Appl. Cryst.* **19**, 105 (1986).
(S2) A. Altomare, *et al.*, *J. Appl. Cryst.* **27**, 435 (1994).
(S3) P. W. Betteridge, J. R. Carruthers, R. I. Cooper, K. Prout, D. J. Watkin, *J. Appl. Cryst.* **36**, 1487 (2003).
(S4) R. I. Cooper, A. L. Thompson, D. J. Watkin, *J. Appl. Cryst.* **43**, 1100 (2010).